

The Scintillation Light Yield per MeV of Deposited Energy in CF₄ Using a Photosensitive Detector

Physics MQP-GSI-0803

Author: Matthew R Rumore

Advisor: Germano S Iannacchione

Keywords:

1. Scintillation Light Yield
2. Gas Electron Multiplier (GEM)
3. Photosensitive Cathode
4. Carbon Tetrafluoride (CF₄)

Table of Contents

Table of Figures.....	3
Abstract.....	4
Chapter Summaries.....	5
Introduction	6
What is the process of Scintillation?.....	6
Cherenkov Radiation and the Hadron Blind Detector	8
Scintillation Light Yield per MeV	10
Gas Electron Multipliers (GEMs).....	12
Geometry of a GEM	12
GEM Gain	13
Triple GEM Stack and a Photosensitive Cathode.....	15
The Apparatus.....	17
Experimental Background and Setup.....	20
The Energy Deposited	20
SBD Timing Signal.....	21
The Scintillation Light Yield.....	22
Geometric Acceptance.....	22
Quantum Efficiency.....	23
Transparencies.....	25
Collection Efficiency.....	26
Calibrations	30
Procedure.....	35
Results and Calculations	38
The Energy Deposited	39
Scintillation Light Yield.....	40
Geometric Acceptance.....	41
Scintillation Light Yield per MeV of Deposited Energy	42
Conclusion.....	45
References	46

Table of Figures

FIGURE 1: SCINTILLATION ON THE LEVEL OF AN ELECTRON.....	6
FIGURE 2: SPECTRUM OF SCINTILLATION LIGHT EMITTED BY CF_4	7
FIGURE 3: THE GEOMETRY OF CHERENKOV LIGHT	8
FIGURE 4: ILLUSTRATION OF USE AND GEOMETRY OF A GEM	12
FIGURE 5: CROSS-SECTION OF A GEM.....	13
FIGURE 6: SETUP OF THE APPARATUS	17
FIGURE 7: GEOMETRY OF THE CONIC RAY.....	18
FIGURE 8: THE BRAGG CURVE	21
FIGURE 9: MONTE CARLO SIMULATIONS FOR THE GEOMETRIC ACCEPTANCE	23
FIGURE 10: QUANTUM EFFICIENCY MEASUREMENT.....	25
FIGURE 11: TRANSMITTANCE OF CF_4	26
FIGURE 12: COLLECTION EFFICIENCY.....	27
FIGURE 13: OPTIMIZATION OF COLLECTION EFFICIENCY	28
FIGURE 14: DRIFT FIELD OPTIMIZATION	29
FIGURE 15: CALIBRATED LIGHT SOURCE	29
FIGURE 16: SBD CALIBRATION	31
FIGURE 17: PREAMPLIFIER CALIBRATION	32
FIGURE 18: GAIN CALIBRATION	33
FIGURE 19: ELECTRIC FIELDS OF GEM STACK.....	36
FIGURE 20: SIGNALS RECEIVED AND PULSE HEIGHT DISTRIBUTION	38
FIGURE 21: RANGE-ENERGY CURVE	39
FIGURE 22: FITTING METHOD	41
FIGURE 23: GEOMETRIC ACCEPTANCE CHECK	42
FIGURE 24: MEAN SIGNAL OUTPUT AGAINST THE ENERGY DEPOSITED	42
FIGURE 25: ABSOLUTE SCINTILLATION LIGHT YIELD PER MEV OF DEPOSITED ENERGY	43

Abstract

Scintillation light is produced by the energy deposited by ionizing particles in certain gases such as carbon tetrafluoride (CF_4). This process is important for the Hadron Blind Detector (HBD) at the Pioneering High Energy Nuclear Interaction Experiment (PHENIX) at the Relativistic Heavy Ion Collider (RHIC) because scintillation light is a background to the signal being detected. We have measured the scintillation light yield in CF_4 using alpha particles emitted by an Americium-241 (^{241}Am) source. As alpha particles traverse a known distance in the gas, they deposit a given amount energy and produce scintillation light. This light was detected using a cesium iodide (CsI) coated Gas Electron Multiplier (GEM) which produces photoelectrons. The photoelectrons were amplified by a triple GEM detector and the total charge was measured using a charge sensitive preamplifier and output to a digital oscilloscope and ROOT program. The energy deposited in the gas by the alpha particle was measured using a silicon surface barrier detector (SBD). We have determined that the scintillation light yield in CF_4 is 314 ± 15 photons per MeV of deposited energy over a solid angle of 4π , with a quantum efficiency of $27 \pm 3\%$ and a collection efficiency of $66 \pm 6\%$.

Chapter Summaries

Introduction

This chapter explains the process and various properties of scintillation light. This light affects the measurement of Cherenkov particle detectors using photon detectors, such as the HBD. Cherenkov radiation and detectors are briefly discussed. A brief explanation of the experiment ends of the chapter.

Gas Electron Multipliers (GEMs)

This chapter is an overview of the geometry, use, and various properties of a single GEM and a triple GEM stack, which are fundamental to the experiment.

The Apparatus

A description of the apparatus used to measure the scintillation light yield per MeV of deposited energy.

Experimental Background and Setup

Here is a description of the details of the experiment and the efficiencies that affect the measurement. I will present a description of how the experiment measures the amount of scintillation light produced per *MeV* of deposited energy.

Procedure

A detailed procedure is given in this chapter.

Results and Calculations

This chapter explains the results of the experiment detailed in the procedure. The obtained results are described separately and related to the final quantitative measurement.

Conclusions

Finally, the experiment is summarized, concluding the report.

Introduction

What is the process of Scintillation?

Scintillation is the process in which photons are emitted due to the ionization of a transparent material, the scintillator. This ionization is achieved through the radiation emitted by electromagnetic waves or particles, minimally ionizing particles (MIPs), or highly ionizing particles (HIPs). The amount of scintillation light produced is dependent on the amount of energy deposited into the scintillator which is directly related to the energy deposited by each particle or the frequency of the wave, rather than the number of individual particles or intensity of the waves. In this experiment, we quantify the amount of scintillation light produced, N_γ , due to the amount of energy deposited into the scintillator, E , over a 4π solid angle. Alpha particles, a type of MIP, were used to scintillate carbon tetrafluoride (CF_4) gas. There exists a large variety of other scintillators, e.g. organic materials, inorganic materials, gasses, crystals, as well as others. Due to the nature of the experiment, I will limit the paper to ionizing particles.

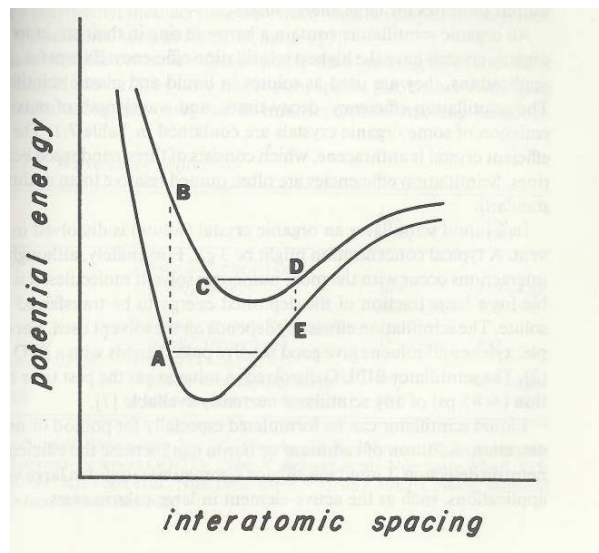


Figure 1: Scintillation on the Level of an Electron. This depicts the potential energy of an electron as a function of the spacing between it and the nucleus. The electron is initially at point A and is disrupted by the energy deposited by the traveling particle. As it changes energy, the spacing changes as depicted. The two different curves shown are two different energy states of the atom. (Fernow 1986)

Fig 1 depicts scintillation on the level of the electron. The scintillator absorbs energy from the particle as the particle travels through it. Assuming the energy is large enough, the materials' electrons

will excite to a higher energy level without changing their interatomic spacing, $A \rightarrow B$ in Fig 1. This phenomenon is due to the Franck-Condon principle which states interatomic distances do not change during molecular electronic transitions, such as this. The electrons are not in equilibrium and proceed to expel vibration energy in the form of photons which is absorbed by the lattice of the molecule, points C and D in Fig 1. The photons are self-absorbed by the scintillator. Quickly after, the electrons will de-excite to a vibrational state of the ground state energy level, again emitting photons, $D \rightarrow E$ in Fig 1. These photons produced are not self-absorbed due to the differences in the two energy levels. This is the scintillation light seen, N_γ . The amount of scintillation light emitted depends on the energy difference of the two discrete energy levels. This de-excitation is very quick; some of the slower reaction times can be $\sim 10 \text{ ns}$ (Fernow 1986).

The process of scintillation will produce a spectrum of light characteristic to the scintillator. Scintillation light is typically in the visible range, but can also be observed in the ultraviolet range as well. CF_4 is found to have a scintillation spectrum seen in Fig 2 (Gernhäuser 1996). This light is in the ultraviolet range. Due to the nature of the CsI photocathode used in this experiment, the only scintillation light measured was around the peak of 160 nm , Fig 2. The standard deviation of the peak is $\sim 5 \text{ nm}$.

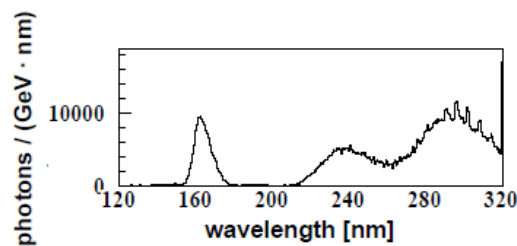


Figure 2: Spectrum of Scintillation Light Emitted by CF_4 . Note the peak centered at 160 nm has a standard deviation of $\sim 5 \text{ nm}$. (Gernhäuser 1996)

The amount of scintillation light produced is linearly dependent on the energy deposited by the ionizing particles. This experiment's purpose is to quantify the scintillation light yield as a function of

the energy deposited into the CF_4 by the alpha particles, dN_γ/dE , over a 4π solid angle. With some adjustment, this experiment can be applied to different gaseous scintillators, such as Argon.

Cherenkov Radiation and the Hadron Blind Detector

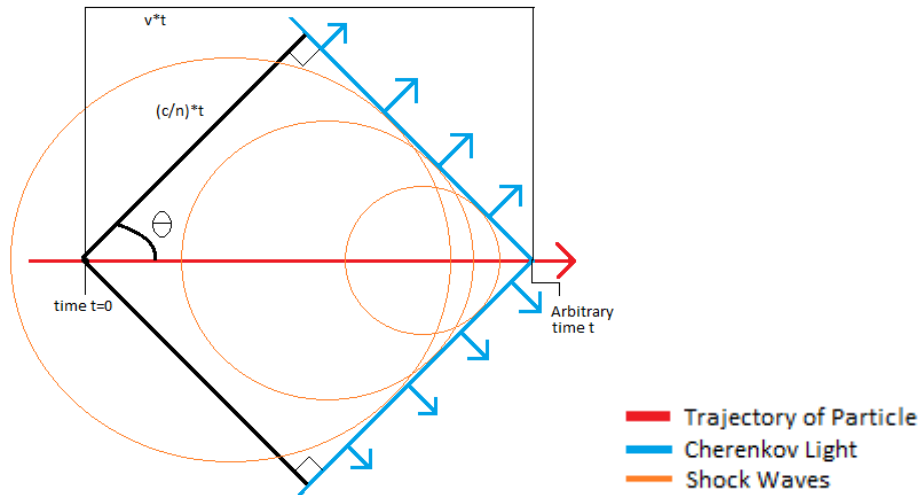


Figure 3: The Geometry of Cherenkov Light. The blue lines represent the Cherenkov wave front which moves in the direction of the blue arrows at an arbitrary time t . The red lines are the trajectory of the charged particle through the medium. The orange circles represent shock waves created by the particle. (Bock and Vasilescu 1999)

This experiment has a direct impact on the field of particle physics. Particle accelerators, such as the Relativistic Heavy Ion Collider (RHIC) located at Brookhaven National Laboratory (BNL), make use of Cherenkov radiation expelled during particle collision experiments, such as the Pioneering High Energy Nuclear Interaction Experiment (PHENIX), to identify a variety of subatomic particles. Cherenkov radiation is emitted as a charged particle travels through an insulator or a dielectric material faster than the speed of light would in that medium. This radiation is emitted in a conic shape and details about the geometry can be illustrated in Fig 3 (Bock and Vasilescu 1999).

The speeding charged particle creates electromagnetic shock waves, disrupting the electromagnetic field of the medium, also referred to as the detector gas or radiator. This will displace the electrons of the material about the particle's trajectory, polarizing the molecules of the radiator. Once the electromagnetic disruption has past, the molecules will quickly revert to equilibrium, emitting photons.

These photons would normally destructively interfere with each other, but because the charged particle is moving faster than the speed of light, the photons will constructively interfere creating a moving wave front, the Cherenkov wave front. This wave front's geometric properties are dependent on the speed of the particle along its trajectory, $v_{particle}$.

The speed of light in the medium, v_{light} , is defined by

$$\frac{c}{n} = v_{light} < v_{particle}$$

where c is the velocity of light in a vacuum and n is the index of refraction of the medium. As seen in Fig 3, the shape of the wave front with respect to the particle's trajectory can be calculated,

$$\cos \theta = \frac{v_{light}}{v_{particle}} = \frac{c}{n * v_{particle}} = 1/n * \beta$$

where β is the ratio of c to $v_{particle}$ and θ is the half-angle of the charged particle's trajectory to the tangent of the wave front in all directions. By measuring the angle of the wave front and independently measuring the momentum of the particle, PHENIX is able to derive the mass of the particle and thus identify the charged particle.

There are a variety of Cherenkov detectors in use and new detectors are being developed. Most Cherenkov detectors are Ring Imaging Cherenkov (RICH) detectors. There are a few varieties of RICH detectors, but the most common use a position sensitive planar photon detector to construct a ring of a certain radius which depends on θ . These detectors generally collect photons with the use of well positioned mirrors. A RICH detector would be nearly impossible to implement at PHENIX due to the use of mirrors and windows. To address these issues, the Hadron Blind Detector (HBD) has been in development and used for the past 10 years. It has collected data for PHENIX during the past couple of runs at RHIC.

The HBD is similar to a proximity-focusing Cherenkov detector, which uses the Cherenkov angle and the volume of gas within the detector to construct an annulus with a specific radius. As opposed to a typical RICH detector, the HBD uniquely lacks windows and mirrors to accommodate the geometry and limitations of PHENIX. The light produced by the Cherenkov radiation is directly collected by a number of triple gas electron multiplier (GEM) stacks which surround the active volume of the detector. “Blobs” of charge are created by the use of the triple GEM stacks. Each GEM stack consists of a mesh and three GEMs. The top GEM is gold plated and coated with a small layer of cesium iodide (CsI) to act as a photo-sensitive cathode. Due to the photoelectric effect, the CsI photocathode produces photoelectrons as photons are absorbed. The photoelectrons are amplified by the GEM stacks resulting in a positional map of the blobs of charge. The net charge of each blob is quantified by a number of small readout pads underneath each GEM stack, approximately three readout pads per GEM stack. CF_4 is the detector gas used in the HBD. Another noteworthy accomplishment of the HBD is due to the operational requirements of the triple GEM stack; it is blind to the signals of the hadrons produced by the heavy Au-Au ion collisions. Further details surrounding the HBD will not be discussed in this paper (Azmoun et al. 2004).

Scintillation Light Yield per MeV

The HBD used at RHIC is a perfect example of a Cherenkov detector in need of the quantitative result of dN_γ/dE over a 4π solid angle. The HBD is highly UV sensitive and the scintillation light is a background to the Cherenkov signal. The scintillating gas is also the radiator for the HBD. By the nature of Cherenkov radiation, the process of scintillation will occur while the particle travels through the radiator and directly interferes with the Cherenkov signal. The scintillation light yield per MeV of deposited energy over a 4π solid angle was quantified in CF_4 so it may be analytically removed from the Cherenkov signal received from the HBD.

The method used to measure N_γ is very similar to how the HBD measures the Cherenkov light. Alpha particles produced by an ^{241}Am source traveled through a CF_4 environment to produce scintillation light. The amount of scintillation light emitted was measured using a CsI photosensitive cathode evaporated onto a triple GEM stack. The photocathode produced a number of photoelectrons in direct relation to the amount of scintillation light absorbed. The photoelectrons were amplified by the triple GEM stack and the signal was collected onto a readout pad. The signal traveled from the readout pad to a charge sensitive preamplifier with a very sensitive feedback capacitor. This signal was simultaneously measured by a digital oscilloscope and a ROOT data collection program to collect a pulse height spectrum of the scintillation light produced by the alpha particles. The amount of energy deposited by the alpha particles was simultaneously measured by the use of a Silicon surface barrier detector (SBD).

The resulting pulse height spectrums and amount of energy deposited into the gas were differentially analyzed. The separate pulse height spectrums were collected in two independent ways. The data collected by the digital oscilloscope used an experimentally calculated gain of the triple GEM stack to determine N_γ . The second method consisted of fitting the pulse height spectrum collected by the ROOT program to a curve comprised of a convoluted polya gain distribution due to the GEM gain fluctuations, a Gaussian distribution due to the pedestal of the signal, and a Poisson distribution due to the number of photoelectrons expelled by the photocathode, N_{pe} . With certain knowledge of the photocathode, N_γ can be derived from the Poisson distribution.

To differentially analyze the data, the scintillation light produced by each incident alpha particle must be measured simultaneously with the amount of energy deposited by that corresponding particle. To achieve this, the SBD produced two signals for each alpha particle: a timing signal and an energy signal. The timing signal was used to trigger the oscilloscope and ROOT program. Both data collecting methods measured the energy of the particle as well as the pulse height spectrum.

Gas Electron Multipliers (GEMs)

GEMs are an extremely critical tool used in this experiment and it is therefore necessary to understand the operation of a GEM and a GEM stack. GEMs were invented at European Council for Nuclear Research (CERN) by Fabio Sauli (1997). They can be used as gaseous ionization detectors and are powerful tools used in nuclear and particle physics as well as radiation detection. GEMs can also be used instead of, or in addition to other ionization detectors such as multi-wire proportional chambers. Unlike other detectors, GEMs are operationally simpler, much more resilient to unexpected discharges, and are ultimately used in this experiment, as well as in the HBD, for their favorable size (Sauli 1997). Through simple calculations, we are able to calculate the scintillation light yield over a 4π solid angle from any solid angle covered by the GEM.

Geometry of a GEM

An illustration of the geometry and use of a GEM is depicted in Fig 4. GEMs are manufactured to an array of sizes, most commonly $3 \times 3 \text{ cm}^2$ and $10 \times 10 \text{ cm}^2$. A GEM is a device that may first appear as a thin sheet of copper, but is in fact is made of two sheets of copper separated by a strong insulator such as Kapton.

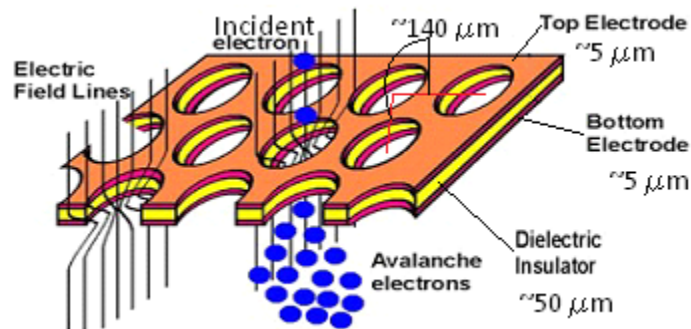


Figure 4: Illustration of Use and Geometry of a GEM. The incident electrons drift into the top hole. Due to the high electric field, charge is gained and exits the bottom hole. The thickness of the top and bottom electrode is $\sim 5 \mu\text{m}$ and the dielectric insulator is $\sim 50 \mu\text{m}$ thick. The holes are spaced $\sim 140 \mu\text{m}$ on center. (Azmoon et al 2010)

Typically each layer of copper is $\sim 5 \mu\text{m}$ thick and the insulator is typically manufactured to a thickness of $\sim 50 \mu\text{m}$. These three layers are perforated usually by an acid etching process to create two

conic shaped holes on each side of the GEM, ultimately creating holes or channels of an hourglass shape. The geometry of a typical hole is illustrated in Fig 5. Fig 5 also shows a generic diagram of equipotential lines and electric potential lines affecting the holes of an operational GEM. The top or entry channels have a slightly larger diameter than the bottom or exiting channels to improve on dielectric rigidity. The hourglass holes are typically $\sim 80 \mu\text{m}$ in diameter on top, $\sim 60 \mu\text{m}$ in diameter on the bottom, and $\sim 50 \mu\text{m}$ in diameter in the middle. They are evenly spaced by $\sim 140 \mu\text{m}$ throughout the entire active area of the GEM as seen in Fig 4. The sizes of the holes and their pattern vary across a GEM due to the acid etching process. These unintended differences will slightly vary the gain across the GEM; however, the absolute gain is measured as a whole, so the variations from hole to hole may be ignored (Bachmann et al. 1999).

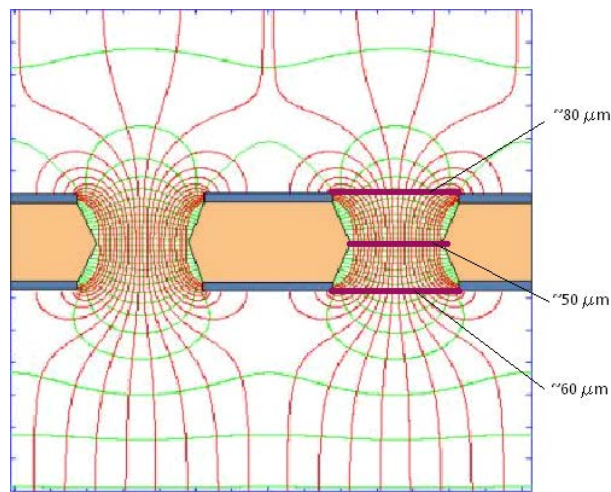


Figure 5: Cross-section of a GEM. The green lines displayed are equipotential lines and the corresponding electric field lines are shown as well in red. Typically, the top hole will have a diameter of $\sim 80 \mu\text{m}$, while the bottom hole will have a smaller diameter, $\sim 60 \mu\text{m}$. The middle of the hourglass shape typically has a diameter of $\sim 50 \mu\text{m}$. (Azmon et al. 2010)

GEM Gain

The gain of a GEM is the multiplicative factor that multiplies an initial amount of charge over the active area of the GEM. Gain is produced by creating a strong potential difference, ΔV , between the two copper sides, $\sim 500 \text{ V}$ over a distance of $\sim 60 \mu\text{m}$ for a gain of 10^3 in CF_4 . This will create a strong electric field in and around the GEM. At a 200 V difference, the strength of the central field line can

reach up to $40 \text{ kV}/\text{cm}$. Due to these strong electric fields, it is imperative there are no sharp or jagged edges on or very close to the active area of the GEM. As ionization occurs above the GEM, or the drift gap, electrons will drift into the channels creating an avalanche of charge exiting the area of a high electric field. The ionization is created by additional primary ionization. There exists some level of secondary ionization and other effects such as diffusion which will affect the gain, but these are typically considered negligible. This new avalanche of charge is a “blob” of electrons which is an amplification of the original charge (Sauli 1997).

There are a number of operating parameters that affect the gain of a GEM. A GEM is usually operated below a mesh to control the electric field of the drift gap, the drift field. This can considerably affect the gain. If the potential of the mesh is set higher than the top of the GEM, electrons will be directed towards the mesh instead of traveling through the holes, preventing gain. This is called reverse bias. In forward bias, the mesh is set to a lower potential to force the electrons to move towards the GEM holes. ΔV is the most prominent operating parameter that affects the gain. A greater ΔV will result in a higher gain, but it is not unchecked. If it is set too high, the GEM will discharge and may be damaged. If a discharge occurs, the GEM will have to be brought to ground, checked for damage, and high voltage must be reapplied. The gap under the GEM is called the induction gap. The induction field is set to force the electrons away from the GEM and its magnitude is not an important factor.

The amplification across the entire GEM is the absolute gain, or simply the ratio of charge that exits to the charge that entered. Again, ideally the avalanche is created by ionization due to primary electron impact only. The gain of a GEM can be expressed as a Polya distribution, also known as the negative binomial distribution or Pascal distribution,

$$P_{(q)} \cong \left[\left(1 + \theta \right) \frac{q}{\bar{q}} \right]^\theta * e^{-(1+\theta)q/\bar{q}}$$

where q is the number of electrons in an avalanche, \bar{q} is the mean number of electrons in an avalanche, and θ is a parameter. This experiment is only interested in the gain fluctuations allowing us to set $\bar{q} = 1$. The Polya distribution is the discrete analog distribution of the exponential distribution and because of this relation it is important to note that if $\theta = 0$, the Polya distribution reverts to an exponential distribution. θ is generally a positive value, but a negative value can occur and tends to be a result of secondary avalanches. This is typically seen in cases where the gas, or scintillator in our case, is not quenched adequately. The physical significance of θ is not fully understood (Va'vra et al. 1993). CF_4 is known to have a positive value for θ , and in this experiment $\theta = 0.38$ (Azmoon et al. 2010).

In addition to the operating parameters, gain is affected by geometric and environmental factors, i.e. pressure, temperature, and oxygen/water levels. The geometry of the GEM, i.e. the inner and outer diameters and the distance between each hole, will affect the gain of the GEM. The size of the active area will affect the total gain due to the larger drift gap. The rate of the incoming ionization also affects the gain of the GEM and if the rate is high enough, the GEM may saturate and will not work as intended. Another prominent property of GEMs is a charge up effect which initially occurs when the voltage is applied. It will first exhibit relatively low gain which will exponentially increase over time. The gain will stabilize and the level of gain achieved is the absolute gain of the GEM. After the gain has stabilized and if a discharge occurs, the charge up effect will not reset. For more information on these properties, see Kozlov (2004).

Triple GEM Stack and a Photosensitive Cathode

As declared in the introduction, a CsI coated triple GEM stack with a mesh was used to amplify the photoelectrons produced. Multiple GEMs may be placed in succession to create a greater absolute gain. The GEMs operate as if they were independent, but their respective gains combine in stages. The stack can be considered a complete unit with a single stage of gain (Sauli 1997). The space between each GEM is called a transfer gap and the transfer field in between each GEM is set to force electrons to

the next GEM. The first transfer field affects the transfer efficiency, which is a new property which affects the electrons amplified between each GEM. The use of the evaporated CsI coating as a photocathode introduces an additional two factors as well: the extraction efficiency and the quantum efficiency. The extraction efficiency and the transfer efficiency are lumped together into the collection efficiency, the ratio of photoelectrons produced by the photocathode of known quantum efficiency to the number of electrons amplified and collected in the induction gap. The properties of the collection efficiency and how it affects the measurement is explained in the Collection Efficiency subsection of the Experimental Background and Setup section. The quantum efficiency is the probability a photoelectron is emitted by the photocathode when it absorbs a photon. It is also explained in the Experimental Background and Setup section in the subsection Quantum Efficiency.

The Apparatus

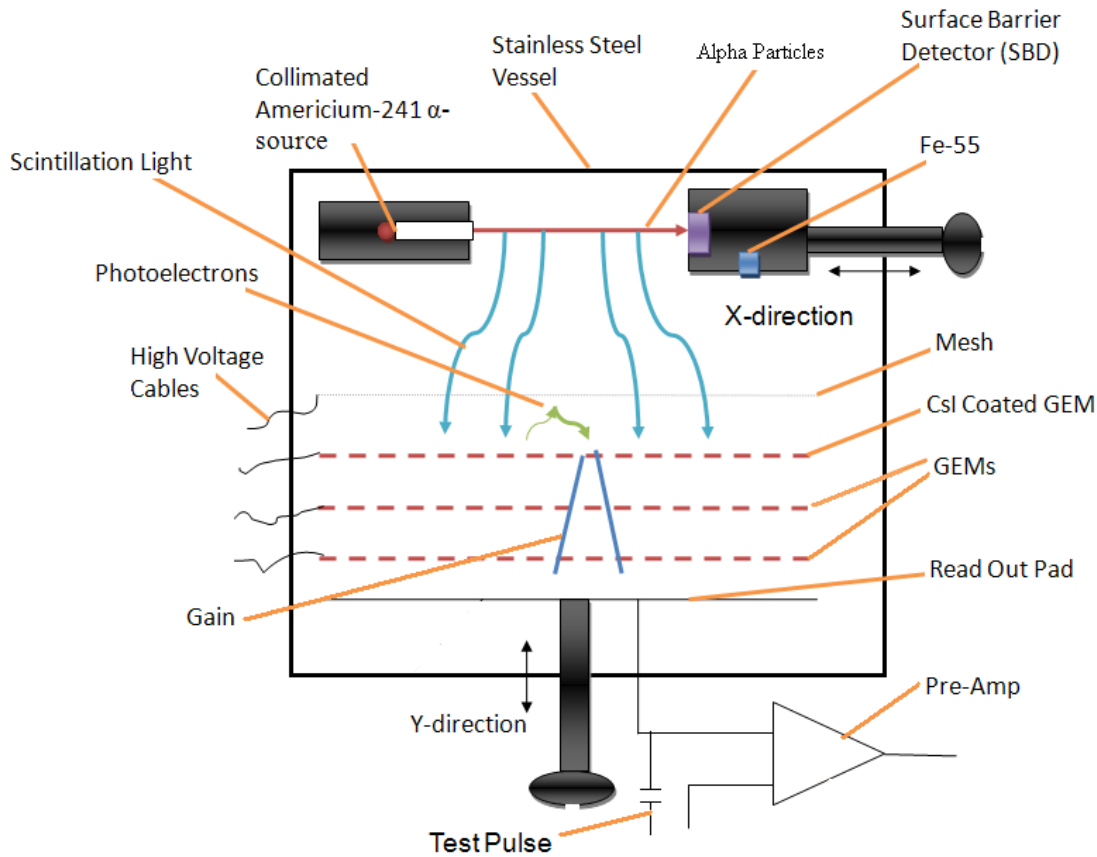


Figure 6: Setup of the Apparatus.

The apparatus used in the experiment is shown in Fig 6. The entire experiment was contained in an air tight stainless steel box, or “the cube”, with a volume of 7.7 L. A pressure and temperature sensor was present in the cube. The cube was able to be filled with gas or placed under vacuum and could also switch between the two without exposing the environment to air. The cube was first placed under vacuum for ~15 hours to remove as much water, oxygen, and air before filling it with CF_4 . The gas flow was set at a high rate to circulate the CF_4 well enough to maintain low levels of water and oxygen to better stabilize the gain and ensure the best measurement of the pulse height spectrum. The gas flowed through a gas analysis system to measure the levels of water and oxygen. The gas would then flow to atmosphere through a bubbler. The level of the water and oxygen were optimally ~10 ppm each.

Inside the cube, the CsI coated triple GEM stack with a mesh was placed on a movable platform which allowed it to move towards or away from the trajectory of the alpha particles, which is defined as the Y-direction. This changed the geometric acceptance and will not change N_γ over a 4π solid angle. The GEM stack consisted of three $3 \times 3 \text{ cm}^2$ GEMs. The top GEM was gold plated and coated with $\sim 350 \text{ nm}$ of CsI to act as a photosensitive cathode. Each side of each GEM was attached to a voltage divider to easily place high voltage on them. The mesh above the GEM stack had a separate high voltage input. A readout pad collected the resulting blob of amplified charge under the GEM stack. The signal was sent to a charge sensitive pre-amplifier containing a 1.262 pF feedback capacitor and its output was collected on a digital oscilloscope and a ROOT data collection program. These devices collected the pulse height distribution of the peak of the signal received which directly corresponded to N_γ .

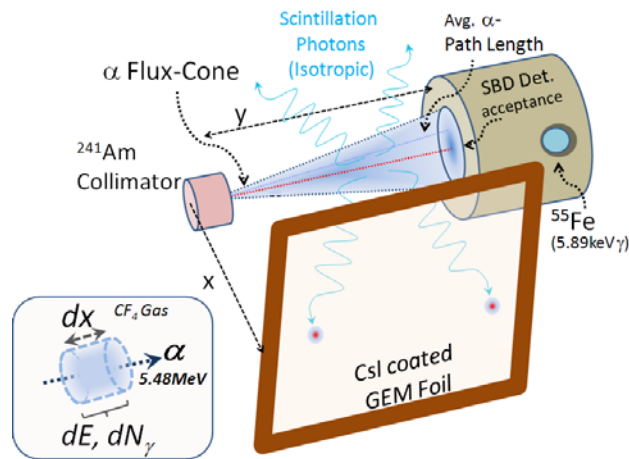


Figure 7: Geometry of the Conic Ray. This illustrates the geometry of the conic ray produced by the ^{241}Am and collimating cylinder. The average path length of the alpha particles is shown as well. The smaller figure describes how we can differentially calculate dN_γ/dE with this setup of the experiment. (Azmon et al. 2010)

Alpha particles are used as a source of ionization to scintillate the CF_4 . They emanated from a radioactive isotope, Americium-241 (^{241}Am). The alpha particles first traveled through a collimating cylinder to direct their paths creating a conic ray, Fig 7. After traversing the gas, each particle was absorbed by a Silicon SBD to measure the residing energy of each incident alpha particle. It also produced

a timing signal to trigger the oscilloscope and data collection program. The energy signal was collected on the digital oscilloscope. The SBD was mounted on a second movable plunger to vary the distance between the SBD and the ^{241}Am source, the X-direction. By doing so, we were able to change the amount of energy deposited into the gas by the particles. If the X-plunger was fully pushed in, the Iron-55 (^{55}Fe) source would be positioned above the GEM stack allowing us to experimentally measure the gain of the GEM stack without exposing the environment to air.

Experimental Background and Setup

There are two major components to quantifying the scintillation light yield per MeV of deposited energy: the amount of scintillation light emitted due to a particle, N_γ , and the amount of energy deposited by the particle, E . These quantities were measured separately and simultaneously to differentially analyze dN_γ/dE over a 4π solid angle. The type of particle initiating scintillation does not affect dN_γ/dE because it is an inherent property of the scintillator. There are a number of efficiencies which need to be accounted for to calculate dN_γ/dE over a 4π solid angle. The efficiencies and how they relate to the inner workings of the experiment will be discussed in this section. This experiment can be implemented to quantify dN_γ/dE for other radiating gases, e.g. ArCO₂ 70/30.

The Energy Deposited

The alpha particles used in this experiment to scintillate the CF₄ were emitted by a radioactive isotope, ²⁴¹Am. The source was placed in a collimating cylinder to create the geometry of a conic ray, Fig 6. Each incident particle will have an initial energy of $5.486 MeV$, E_i , due to the inherent property of ²⁴¹Am (Leo 1994). The energy deposited into the gas, E , was calculated by the law of energy conservation, such that at any point

$$E_i = E_F + E$$

where E_F is the energy of the particle at the final point of its trajectory. The alpha particle will not lose energy when traveling through a vacuum.

The silicon SBD was used to measure E_F of each incident alpha particle. As the incident alpha particle strikes the SBD, the silicon is penetrated producing holes in the silicon and a number of free electrons. These electrons are caught by an electric field and collected to cause a net charge. This

charge induces a bias voltage across a pair of electrodes within the SBD. The resulting voltage difference and the net charge of the free electrons are linearly related and the SBD will output the quantified charge of the incident alpha particle (Gotoh and Takagi 1964). The SBD was placed on a moveable platform to vary the particles' trajectories, and thus directly affecting E . The closer the SBD is to the ^{241}Am , the less energy deposited into the CF_4 .

The alpha particles deposited an amount of energy in relation to the distance it traveled as defined above. The loss of energy by an ionizing particle is dependent on the length the particle travels, the medium in which it travels, and other environmental factors such as pressure and temperature. Notice the type of particle does not affect E : it is only necessary for the particle to possess the energy to scintillate the medium. The relation of energy lost by the particle against the distance traveled in the medium is described by the Bragg Curve. This curve is quite distinctive and an example is seen in Fig 8. The tail of the Bragg Curve is not as well defined as depicted and more information on the subject can be found in Leo (1994).

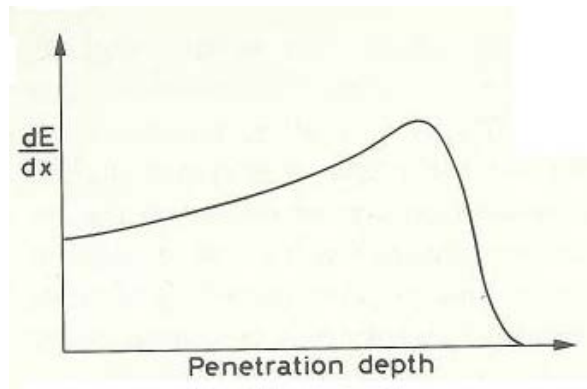


Figure 8: The Bragg Curve. This is an example of the Bragg curve, the rate at which the particle expels energy as a function of the length it has traveled within a medium. The tail end of the curve is not as well defined as depicted. (Leo 1994)

SBD Timing Signal

In addition to the energy signal, the SBD produced a timing signal coincident with each absorbed incident alpha particle. The signal was used to create a trigger pulse to trigger the oscilloscope and

ROOT program which independently collected the signal received from the charge sensitive preamplifier. The pulse continued until the SBD energy signal returned to its pedestal. This presented a method to measure the pulse height distribution and the energy of each incident alpha particle simultaneously allowing us to differentially analyze the independently measured data.

The Scintillation Light Yield

Scintillation light was the product of the excitation and de-excitation of the surrounding molecules as the alpha particles deposited energy into the scintillator. This light propagates in all directions from the particle's trajectory and N_γ is dependent on E . There are a number of inefficiencies and corrections that accompanied the measurement of N_γ over a 4π solid angle.

The most apparent correction needed is how to measure N_γ in all directions, or the geometric acceptance. There are a few other efficiencies that affected the signal produced by the illuminated CsI photocathode and amplified by the GEM stack: the quantum efficiency, the collection efficiency, and the optical transparency of the GEM, mesh, and scintillator. The quantum efficiency determines the number of primary photoelectrons produced by the CsI photocathode after absorbing the scintillation light. The collection efficiency is the ratio of the number of primary photoelectrons emitted by the CsI photocathode of known quantum efficiency and the number of photoelectrons amplified and collected onto the readout pad. The transparency efficiencies are due to the optical transparency of the GEM and mesh. Light may be absorbed by the scintillator as well. In the next section these efficiencies will be discussed and how they are related to N_γ .

Geometric Acceptance

A solid angle is a two dimensional angle in three dimensional space, i.e. a 4π solid angle is an entire sphere. The photocathode can only absorb the light which falls within its solid angle. By dividing the data by the geometric acceptance of the setup, we calculated the amount of scintillation light over a

4π solid angle. With the use of computational software, the geometric acceptance was calculated using two separate Monte Carlo simulations, Fig 9.

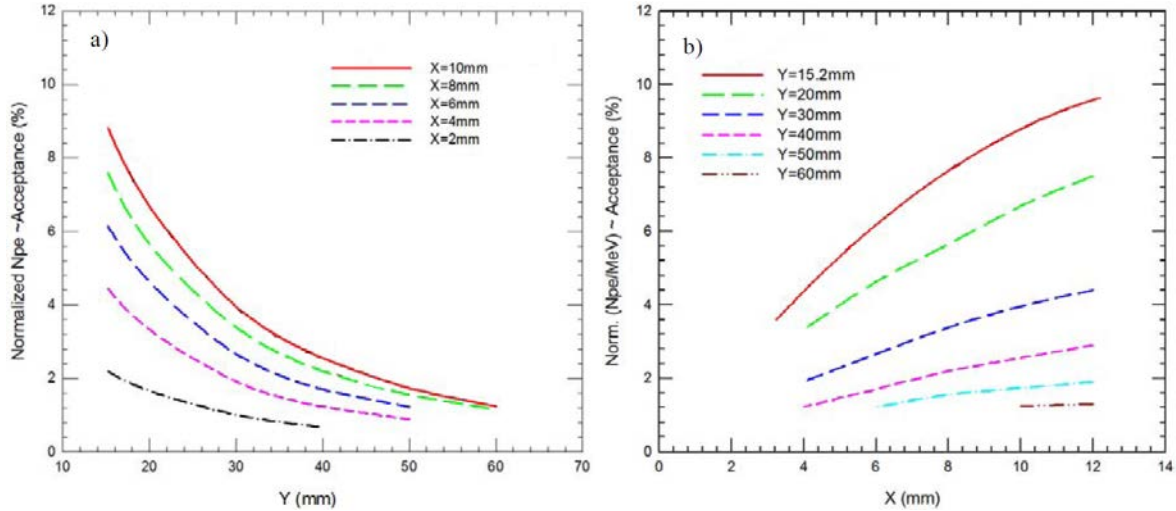


Figure 9: Monte Carlo Simulations for the Geometric Acceptance. Fig 9a shows the geometric acceptance of various X-distance as a function of the Y-distance. Fig 9b shows the geometric acceptance of various Y-distance as a function of the X-distance (Azmoon et al. 2010).

Fig 9a shows the calculated geometric acceptance of discrete X-distances while varying the Y-distances. The other simulation, Fig 9b, calculated the geometric acceptance of discrete Y-distances while varying X-distances. The statistics used for these simulations were large enough that variational differences were negligible.

Quantum Efficiency

The quantum efficiency of the photocathode is the probability a photoelectron is emitted after light is absorbed. This property is dependent on the energy of the incoming photon, which is dependent on the wavelength of the light. To measure the quantum efficiency of the unknown CsI coated GEM, a parallel plate configuration was utilized and the procedure consisted of two steps. A spectrometer with two holding cells each under vacuum was able to emit incremented wavelengths of light to each cell equally for a known amount of time. The first cell contained a monitor CsI coated photomultiplier tube (PMT) with known quantum efficiency and gain to normalize the intensity of the light throughout the

measurement. The second cell first contained a second CsI coated PMT with a known quantum efficiency and gain to measure the flux of photons received by the each cell.

Once the flux of photons was known for each wavelength, the second PMT was replaced by the CsI coated GEM with unknown quantum efficiency under a mesh. High voltage was applied to the mesh and GEM. There was a small amount of current on the mesh due to the applied voltage which was recorded to correct for the quantum efficiency measurement. The set up was configured to reverse bias forcing the photoelectrons produced to be collected on the mesh. This created a current, I , on the mesh due to the flux of photoelectrons. With the known flux of photons entering the test cell as well as the number of photoelectrons produced by the photocathode, we were able to produce a plot of the probability a photoelectron is emitted by the photocathode as a function of the incoming wavelength, the quantum efficiency. The number of electrons produced is found by

$$t * I = Q$$

where Q is the amount of charge produced over time t . With the known quantum efficiency, we can divide the number of produced photoelectrons by the quantum efficiency to calculate the number of photons which illuminated the photocathode, N_γ . The quantum efficiency of the photocathode used was measured to be $27 \pm 3\%$.

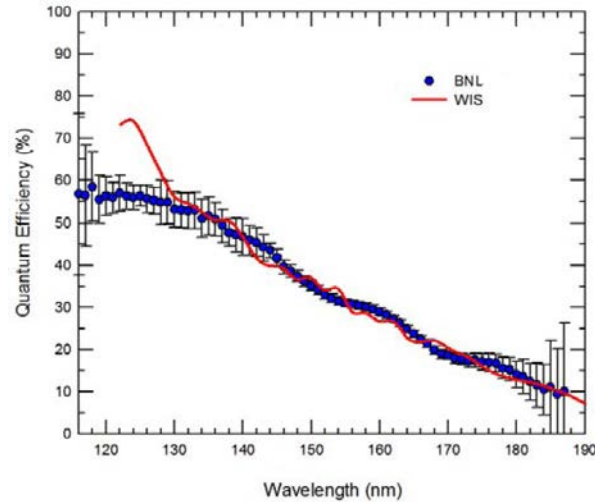


Figure 10: Quantum Efficiency Measurement. This is a typical quantum efficiency measurement of a CsI photocathode used for this experiment. The blue points were measured using a parallel plate configuration. The red line indicates a measurement done at the Weizmann Institute of Science located in Israel (Azmon et al. 2010).

Fig 10 shows a typical quantum efficiency plot of a CsI photocathode used in the experiment. The blue data points are the measured values of the quantum efficiency using the parallel plate configuration. The red line is a measurement of the quantum efficiency obtained by the Weizmann Institute of Science in Israel, which agrees well with our collected data.

The photocathode is highly sensitive around photons of 160nm wavelength, which is important due to the 160nm peak of the spectrum seen in Fig 2. This quantum efficiency is also why the 160nm peak is the only part of the spectrum of to be measured. The scintillation light spectrum consists solely of the 160nm peak until a wavelength of $\sim 220\text{nm}$. The photocathode will produce no photoelectrons at these higher wavelengths, thus making the 160nm peak the contributing source of photoelectrons.

Transparencies

The optical transparencies of the gas, GEM, and mesh will affect the final measurement. The transparencies will detract from the primary signal being collected. As light transverses through a medium, the medium may absorb the light in the form of energy depending on the photons' wavelength. We

are fortunate in this experiment because CF_4 is transparent to the scintillation light created about the 160nm peak.

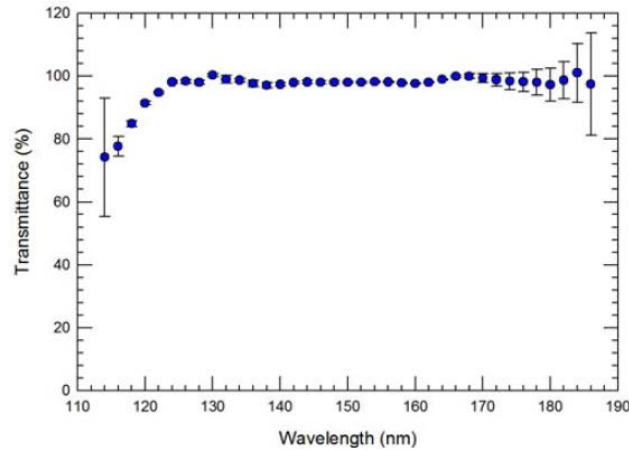


Figure 11: Transmittance of CF_4 . This graphs the transmittance of CF_4 as a function of wavelength. Note that around 160nm the transmittance is practically 100% (Azmoun et al. 2010).

Seen in Fig 11, the percentage of transmitted light as a function of wavelength is shown. Practically all light beyond a 130nm wavelength, CF_4 is fully transparent. As seen in Fig 2, the scintillation light produced by CF_4 is narrowly peaked around 160nm and the transparency of the gas at that wavelength is 100%.

The GEM and mesh possess an optical transparency which will affect the measurement. These were measured by simulation and the GEM transparency was found to be $T_{GEM} = 83\%$ and the mesh transparency was found to be $T_{mesh} = 80\%$. The number of statistics used were large enough that variational differences were negligible.

Collection Efficiency

The collection efficiency is defined to be the ratio of photoelectrons amplified and collected on the readout pad, $N_{collected}$, to the number of photoelectrons emitted by the photocathode for a given quantum efficiency, $N_{produced}$. This efficiency is due to the geometry and operating procedures of the CsI coated triple GEM stack. To calculate this efficiency a calibrated light source was made to illuminate

the CsI coated GEM stack and the number of photoelectrons collected was compared to the number of photoelectrons produced by the photocathode with known quantum efficiency.

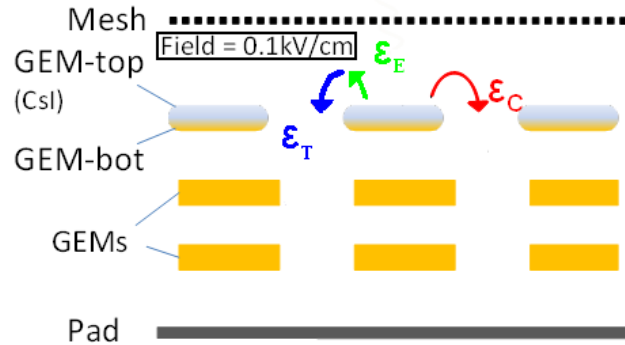


Figure 12: Collection Efficiency. This portrays where the collection, extraction, and transfer efficiency affect the collection of the photoelectrons produced and amplified. The drift field in this example is set to 0.1 kV/cm .

The collection efficiency, ϵ_C , can be factored into two components: the extraction efficiency, ϵ_E , which occurs near the surface of the photocathode, and the transfer efficiency, ϵ_T , which occurs a number of free mean paths away from the surface of the photocathode. Where these efficiencies take effect is depicted in Fig 12 and relate mathematically

$$\frac{N_{collected}}{N_{produced}} = \epsilon_C = \epsilon_E * \epsilon_T$$

ϵ_E is hypothesized to be dependent on the wavelength of the light, the drift field, and backscattering. Backscattering does not occur in a vacuum. ϵ_T is hypothesized to be affected by additional backscattering and possible recombination of electrons onto a GEM surface. Woody et al. (2009) can explain the three efficiencies in more detail. I will briefly explain how the collection efficiency was measured and optimized for this experiment.

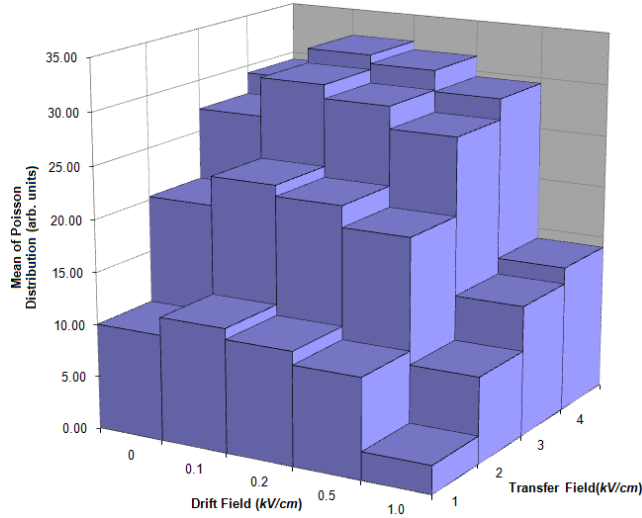


Figure 13: Optimization of Collection Efficiency. This plot shows the signal received from the preamplifier as the drift field and the transfer field were separately varied. The drift field was found to be optimal at 0.1 kV/cm and the transfer field was found to level out.

The optimization of the collection efficiency due to the drift field and first transfer field is an important measurement because it directly affects the number of photoelectrons amplified and collected by the GEM stack. For example, if the drift field is set to reverse bias, no photoelectrons will be amplified and collected on the readout pad because they will be attracted to the mesh. If the field is in forward bias and the drift field is set very high, the electrons will not escape the surface of the photocathode and practically no electrons will be amplified. If the transfer field is set too low, electrons may be lost in travel and not collected by the readout pad. In order to collect and amplify the greatest number of photoelectrons emitted by the photocathode, the output of the preamplifier was measured as a function of the drift field as well as the transfer field, varying each separately and independently, Fig 13. The drift field was optimized more precisely and the results are shown in Fig 14. The optimized drift field was found to be 0.1 kV/cm . The transfer field was set to 3 kV/cm for our experiment. This was also true when photoelectrons are produced by the ^{55}Fe .

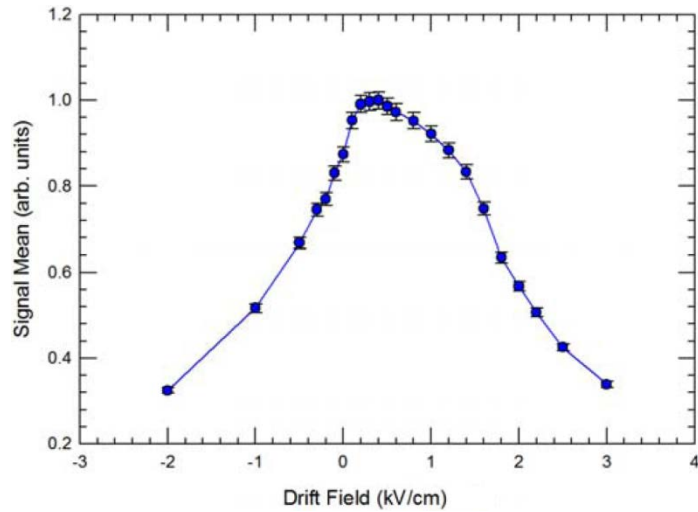


Figure 14: Drift Field Optimization. The plot shown here is the signal received by the preamplifier as a function of the drift field. The drift field was varied from reverse to forward bias and was optimized at 0.1 kV/cm . The points measured are shown in blue and a best fit was applied. (Azmoun et al. 2010)

ε_C was treated as a solitary efficiency and is a function of the parameters and effects of ε_E and ε_T . To measure ε_C , a custom light source was built, shown in Fig 15. The energy deposited by the alpha particles remained constant because of the small distance between the ^{241}Am source and the Silicon SBD.

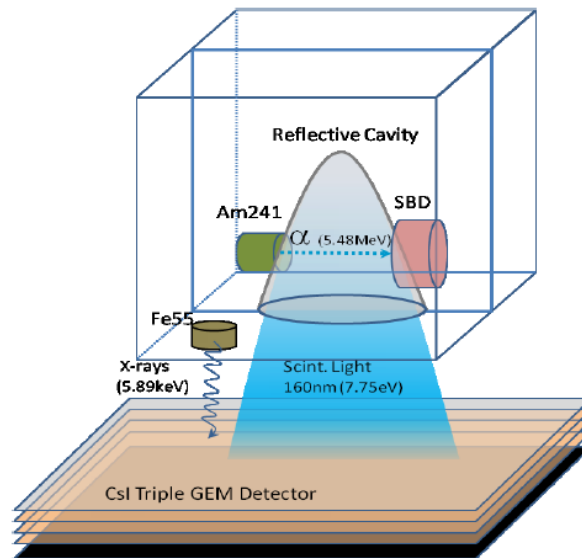


Figure 15: Calibrated Light Source. This is the calibrated light source used to measure ε_C . The alpha particles deposited an amount of energy corresponding to a distance of $\sim 9 \text{ mm}$. The ^{55}Fe was used to calibrate the gain of the GEM and the SBD was used to measure the energy of the alpha particles after they traveled through the gap. (Woody et al. 2009)

The flux of photons produced by the calibrated light source, $N_{\gamma C}$, was measured using a CsI coated PMT with a known gain and quantum efficiency. With this information, we were able to calculate the number of photoelectrons to be produced by the calibrated light source from the CsI coated GEM stack

$$N_{produced} = N_{\gamma C} * T_{mesh} * T_{GEM} * QE_{CsI@160nm}$$

for a known quantum efficiency of the CsI photocathode used, $QE_{CsI@160nm}$. The CsI coated GEM stack with known quantum efficiency was then illuminated by the calibrated light source in CF_4 and a pulse height spectrum to find $N_{collected}$. $N_{collected}$ was measured in a very similar manner to the measurement of dN_{γ}/dE , the difference being the energy deposited was constant. With the measured pulse height spectrum, the same two methods were employed to calculate $N_{collected}$. The first method used an experimentally calculated gain and the second method consisted of using Monte Carlo simulations and chi squared analysis to use the shape of the pulse height spectrum. The results of these two methods were combined with a non-weighted averaged and the error was defined to be half of the difference between the results because it was found to be systematic. The collection efficiency was measured to be $66 \pm 6\%$.

Calibrations

A simple method was used to convert the electronic signals received from the SBD energy signal and the charge sensitive preamplifier to a physically meaningful measurement, i.e. an absolute energy scale and a number of photoelectrons. The signal received in both cases was measured on a digital oscilloscope and by a ROOT computer program in arbitrary units. To achieve this, conversion factors were calculated for the SBD energy signal, the signal received by the preamplifier, and the gain of the GEM stack.

The SBD sent an energy signal to the oscilloscope, ultimately calculating the energy deposited into the gas. A conversion factor was measured so one may convert the raw signal in mV to energy in MeV . The signal attenuation and degradation of the SBD was first measured to correct for any electronic discrepancies by injecting known voltages into the SBD, varying from 20 to 200 mV. To calculate the conversion factor, the apparatus was placed under vacuum allowing the alpha particles emitted to lose no energy while traveling the distance between the SBD and the ^{241}Am source, thus depositing the full 5.48MeV into the SBD. The conversion used is simply the ratio of 5.48MeV to the signal of the SBD while under vacuum. An example of the calibration is seen in Fig 16 and in this example the conversion is $6.919 \times 10^{-3} \frac{\text{MeV}}{\text{mV}}$.

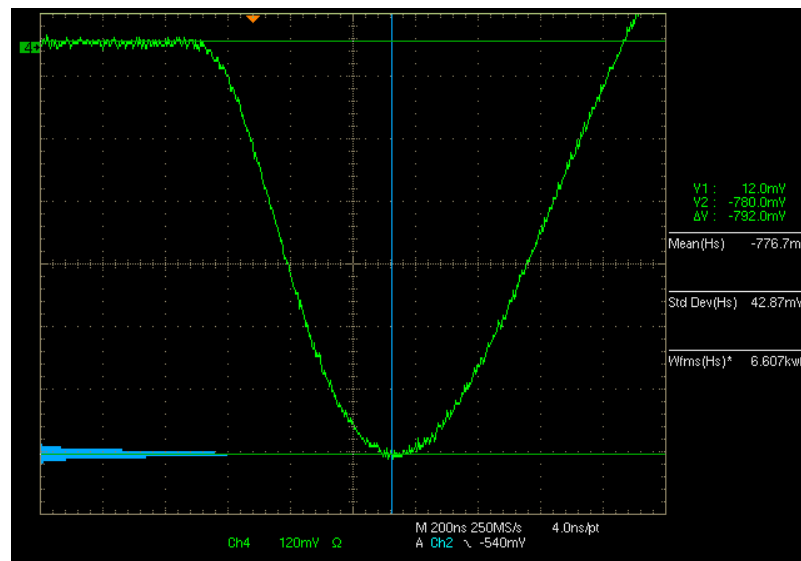


Figure 16: SBD Calibration. This is a screen print out of the digital oscilloscope during an SBD calibration. The difference between the pedestal and the peak of the signal corresponds to 5.48MeV . The blue line is the area in which the histogram collects data. The histogram is seen on the left of the figure.

The charge sensitive preamplifier measured the amount of charge collected on the readout pad and output a corresponding mV signal collected by the oscilloscope and ROOT program. The conversion factor directly converted the signal received by the preamplifier to the absolute charge collected on the

readout pad. This was found by injecting a series of test pulses into the preamplifier. With the resulting signals, we can calculate the amount of charge input into the preamp,

$$q = \frac{VC}{e}$$

where q is the charge injected into it, V is the voltage of the test pulse, C is the capacitance of the feedback capacitor in the preamplifier, and e is the charge of the elementary charge of an electron. As mentioned before, $C = 1.262pF$. An example of this calibration is shown in Fig 17 and a linear fit was used to find the slope of the line. In this example, the conversion factor is $11170.7 \frac{electrons}{mV}$.

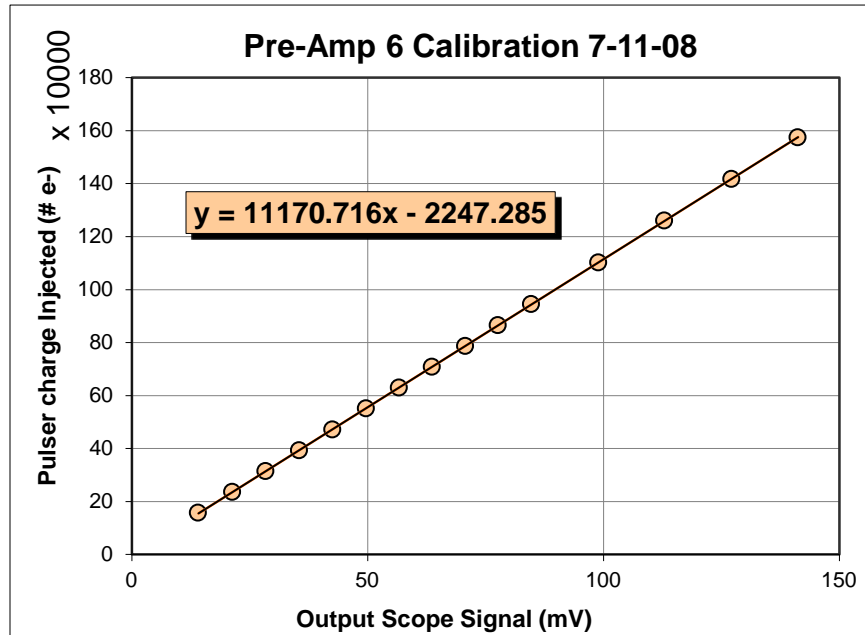


Figure 17: Preamplifier Calibration. This is an example of a preamplifier calibration which allows us to calculate the number of electrons collected on the readout pad directly from the output of the preamplifier. The calibration shown is a graph of the number of electrons injected into the preamplifier due to various test pulses as a function of its resulting output signal.

A final calibration may be needed to convert the signal received on the readout pad to N_{pe} , or the gain calibration. From the calibration of the preamplifier, the charge collected on the readout pad was found, q . With an experimentally calculated gain of the GEM stack, we can find the charge amplified simply by

$$q_{primary} = \frac{q}{g}$$

where $q_{primary}$ is the charge produced by the CsI photocathode and g is the gain of the GEM stack. g was calculated with the use of the ^{55}Fe mounted on the X-plunger. For the calibration, the ^{55}Fe was placed above the GEM stack and a pulse height spectrum was collected and fit to a Gaussian and a Quadratic curve by the ROOT program, Fig 18.

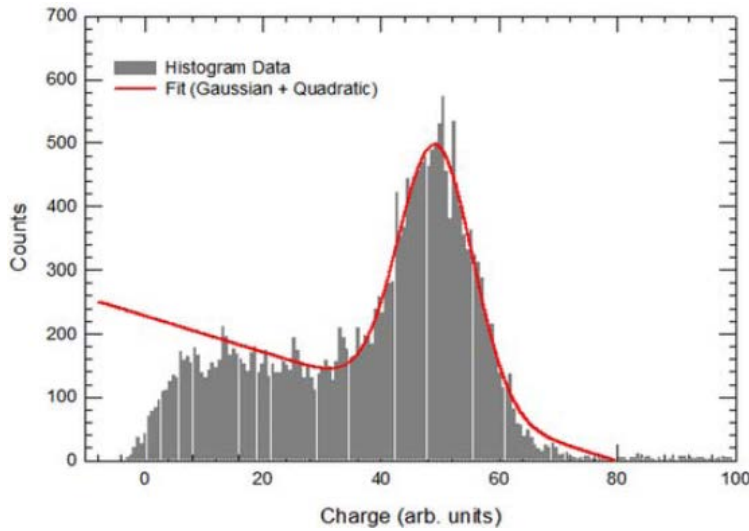


Figure 18: Gain Calibration. This is the pulse height spectrum collected to calculate the gain calibration. The data was fit to a Gaussian and Quadratic curve and the peak of this fit corresponded to 109 photoelectrons. (Azmon et al. 2010)

This pulse height spectrum is the result of the 5.9keV X-rays emitted by the ^{55}Fe source. These X-rays are known to produce 109 primary photoelectrons in CF_4 . The peak of the fit corresponded to 109 primary photoelectrons. With this information, the known quantum efficiency, the preamplifier calibration, and the collection efficiency, we can calculate g from the resulting peak of the pulse height distribution. This was done a number of times to measure the variation of the gain. The gain was found to vary by a maximum of $\pm 5\%$. In this example, the gain calibration is $2.271 \frac{\text{photoelectrons}}{\text{mV}}$.

Once g was found, the calculation of the gain conversion factor is trivial and we are able to convert the output signal of the preamplifier in arbitrary units to the number of electrons produced by the

photocathode. It is important to note the charge found with the help of these calibrations do not include the effects of the collection efficiency, quantum efficiency, or geometric acceptance.

Procedure

The procedure to measure dN_{γ}/dE over a 4π solid angle will be explained with the understanding of the inner workings of the experiment and the quantitative corrections mentioned above. The quantum efficiency of the photocathode was first measured using a parallel plate configuration. Afterwards, the CsI coated GEM was placed delicately into the apparatus in a nitrogen environment glove box and the air tight cube was sealed. The stainless steel cube was then placed under vacuum ~ 15 hours to remove as much water and oxygen. The pressure and temperature were measured constantly throughout the experiment by a LabVIEW program which collected data from the pressure and temperature sensors in the apparatus.

The next day numerous measurements were done before flowing CF_4 into the cube. Any measurement concerning the GEM signal or the SBD energy signal was recorded with the digital oscilloscope and the ROOT data program. The SBD was first positioned far enough away from the ^{241}Am source so no particles were absorbed by the SBD and no voltage was placed on the GEM stack. In this configuration, the SBD energy signal and GEM signal received consisted of noise and a pedestal. The noise was reduced as best as possible and the mean and standard deviation of the noise and pedestal were recorded. These measurements were occasionally reviewed and recorded throughout the procedure to ensure stability and linearly correct for any change.

While still under vacuum, the SBD was placed close to the ^{241}Am source for the SBD calibration, however the source was still a small distance away from the SBD due to the collimating cylinder, the source holder, and the SBD holder, $\sim 3mm$. All alpha particles measured in this configuration resulted in a signal corresponding to its full energy, $5.48 MeV$. The conversion factor was found to directly measure the final energy of the alpha particles from the SBD energy signal. A change in the Y-direction did not affect the energy lost by the alpha particles in vacuum or gas; this affects the geometric

acceptance.

The vacuum was disconnected and gas flowed through the cube to atmosphere through a bubbler. Once the pressure of the cube reached atmosphere, the flow rate was set to create a constant pressure in the cube and the gas was set to flow through the gas analysis system. The data collected by the gas analysis system was recorded by the same LabVIEW program throughout the experiment. While the levels of oxygen and water waned, the final energy of the alpha particles was measured and recorded at various X-distances, an X-scan. The Y-distance does not affect this measurement and was set to be constant during an X-scan.

After the X-scan, high voltage was applied to the GEM stack and the X-plunger was positioned to configure the ^{55}Fe above the GEM stack and the gain of the GEM was monitored by the ROOT data collection program to observe when the charge up effect had ended. The voltages were set to create the electric fields depicted in Fig 19. The transfer fields, induction field, and ΔV of for each GEM are less of an issue because of the gain calibration. In our experiment, ΔV for each GEM was set to 550V.

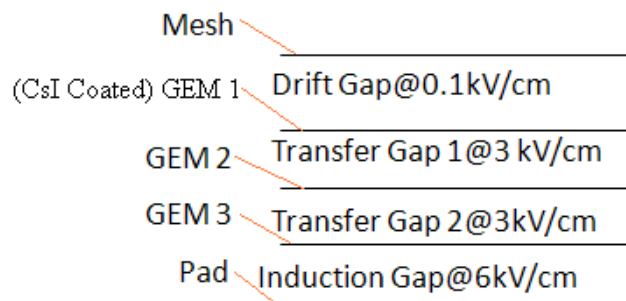


Figure 19: Electric Fields of GEM Stack. The electric fields were set to the values shown. The drift field must be set to 0.1 kV/cm to optimize the collection efficiency.

While the GEM experienced the charge up effect, the charge sensitive preamplifier was calibrated by injecting a variety of test pulses of known voltage into it, resulting in a conversion factor to measure the number of electrons collected onto the readout pad. Once the charge up effect had ceased, the gain of the GEM was calibrated using the ^{55}Fe source.

We were able to measure the scintillation light yield produced by the alpha particles with another X-scan. The SBD was first set to a distance close to the ^{241}Am source; the energy of the alpha particles was known for any corresponding value of the X-distance. Once the distances were set and recorded, the oscilloscope and ROOT program collected a pulse height spectrum of the scintillation light signal received from the preamplifier by creating a histogram of the peak value for approximately 100,000 counts. These histograms were saved on the oscilloscope and ROOT program for later analysis. The SBD is retracted from the source by 2mm and the process is repeated resulting in a different set of pulse height distributions due to the different amount of energy deposited into the CF_4 by the alpha particles. This is repeated until the alpha particles do not reach the SBD, depositing all of their energy into the gas. During the X-scan the energy of the alpha particles was collected to ensure a competent overall result of dN_γ/dE . Once the experiment was complete, the noise and pedestal of the SBD energy signal and GEM signal were retaken to correct for any change during the experiment. To complete the measurement, the gain calibration was also reviewed and recorded.

A systematic test of the measurement was performed by checking the geometric acceptances calculated by the Monte Carlo simulations in Fig 9. During the Y-scan, the X-distance was set to be constant. This was carried out to compare a simulated geometric acceptance to the experimentally calculated number of photoelectrons produced at certain distances. It then followed to set the GEM stack at a constant Y-distance to check the geometric acceptance of an X-scan as well.

A null test was performed to complete the experiment. P-10 (Argon-Methane 90:10) is a gas known not to scintillate. The apparatus was filled with P-10 and no signal was observed from the preamplifier confirming the signal in CF_4 is indeed created by scintillation light.

Results and Calculations

This section will explain the results found from the procedure detailed above and how we calculated dN_{γ}/dE over a 4π solid angle. The final measurement differentially compares the amount of scintillation light produced by the alpha particles and the amount of energy deposited into the CF_4 by these said particles. For our experiment, we measured the quantum efficiency to be $QE = 27 \pm 3\%$ and $\epsilon_C = 66 \pm 6\%$. The transparency of the GEM and mesh are $T_{GEM} = 83\%$ and $T_{mesh} = 80\%$ respectively, the feedback capacitor had a capacitance of 1.262 pF , and the geometric acceptance, A , is determined by Fig 9.

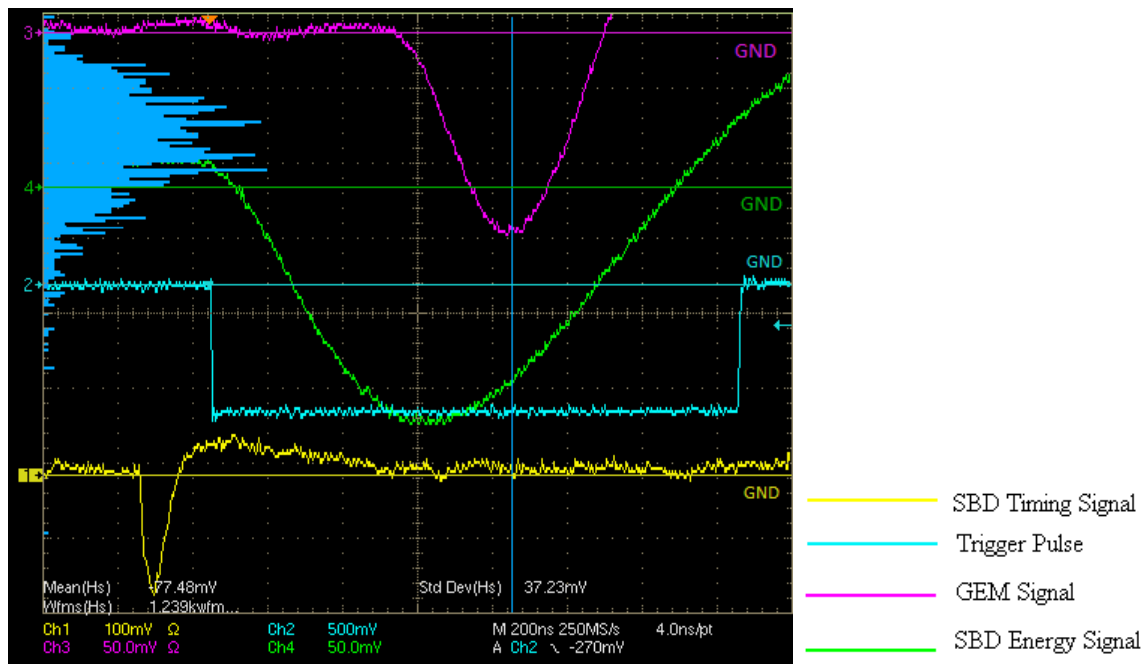


Figure 20: Signals Received and Pulse Height Distribution. This is a screen print out of the digital oscilloscope displaying the signals received from the apparatus. There are four separate signals described by the legend and their corresponding ground levels are shown. The scale for each signal is in the bottom left and the time scale is $200\text{ns per division}$. The vertical blue line is centered on the peak of the GEM signal to collect the pulse height distribution displayed on the left of the screen.

Fig 20 is a screen print out of the digital oscilloscope and presents an example of the signals received from the apparatus. The scale for each signal is given in the bottom left and the time scale is $200\text{ns per division}$. The effect of the pedestal in the GEM and SBD signals can be seen clearly by the

deviation from the ground level. Channel 1 is the SBD timing signal which creates a trigger pulse, Channel 2. As an alpha particle was absorbed by the SBD, the trigger pulse would be signaled until the energy of the SBD returned the pedestal level before the timing signal, thereby signaling the alpha particle has past. Channel 4 is the SBD energy signal and its peak represents the final energy of the absorbed alpha particle. Channel 3 is the GEM signal received from the preamplifier. The vertical blue line was manually set at the peak of the GEM signal to histogram the pulse height distribution of the peak. Typically more counts would be collected than shown in Fig 20 before changing the X-distance.

The Energy Deposited

The amount of energy deposited into the gas by the alpha particles was derived from the range-energy curve shown in Fig 21, which denotes the final energy of a particle as a function of the distance traveled by the particle, or the range. E can easily be derived from this curve by subtracting its initial energy, 5.48MeV , by its final energy.

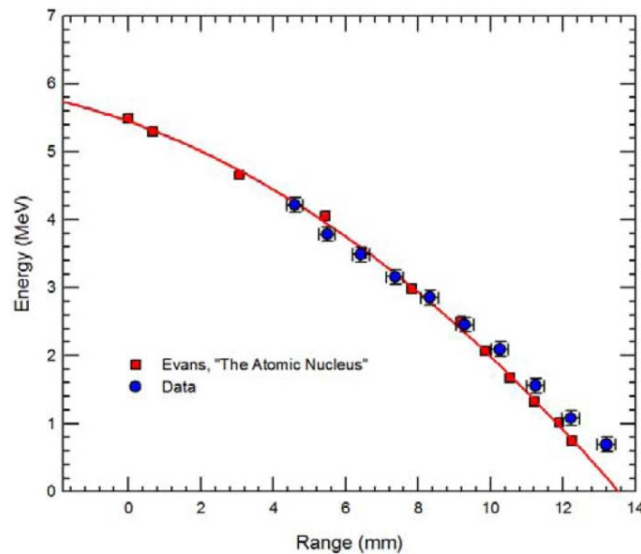


Figure 21: Range-Energy Curve. This depicts the range-energy curve of alpha particles in CF_4 with an initial energy of 5.48 MeV (Azmoun et al. 2010). The blue points describe the energy of alpha particles as a function of the final distance away from the ^{241}Am source. The red points are derived from *The Atomic Nucleus* which were fit to a curve (Evans 1955).

The curve was measured from an X-scan in CF_4 . Our measured values of the particle's final energy in relation to the range of the particle are displayed as blue points. The red points and curve are

derived values of the range-energy curve of alpha particles in air from *The Atomic Nucleus* (Evans 1955). The data measured is in accord with the source and E is known for any X-distance.

Scintillation Light Yield

The scintillation light yield over a 4π solid angle is calculated by

$$N_{\gamma} = \frac{N_{pe}}{QE \times \varepsilon_C \times A \times T_{GEM} \times T_{mesh}}$$

where N_{pe} is the number of primary photoelectrons produced by the CsI photocathode. The set of pulse height distributions collected during an X-scan will allow us to find N_{pe} at their respective values of E . As a reminder, a pulse height distribution was a convolution of a Poisson distribution due to N_{pe} , a Polya gain distribution due to the gain fluxuation where $\theta = 0.38$, and a Gaussian distribution due to the pedestal noise. The spectrums were analyzed by two independent methods, the mean method and the fitting method, both of which were corrected for false zeros created due to the gain fluxuation.

The mean method involved an experimentally calculated gain of the GEM stack to measure N_{pe} directly. Using the digital oscilloscope, the pulse height distribution of the scintillation light was collected and the mean of the output signal was recorded at each X-distance. The mean is then converted to N_{pe} by using the preamplifier and gain calibration

$$N_{pe} = \frac{(Mean) \times (Preamp. Calib.)}{g}$$

Due to the gain fluxuation and pedestal noise, the mean method is not as accurate as the fitting method because the mean may shift. A ROOT program was used to calculate the mean while considering these errors as well, however this is still not as accurate as the fitting method.

The fitting method did not encounter such issues because it was comprised of a chi squared analysis to best fit each measured pulse height distribution to a Monte Carlo simulation which varied

N_{pe} . The Monte Carlo simulations included the broadening effects due to the gain and pedestal noise and an example of a typical fit overlaying the data in Fig 22. The example is formed by ~ 4 photoelectrons produced by the photocathode of known quantum efficiency.

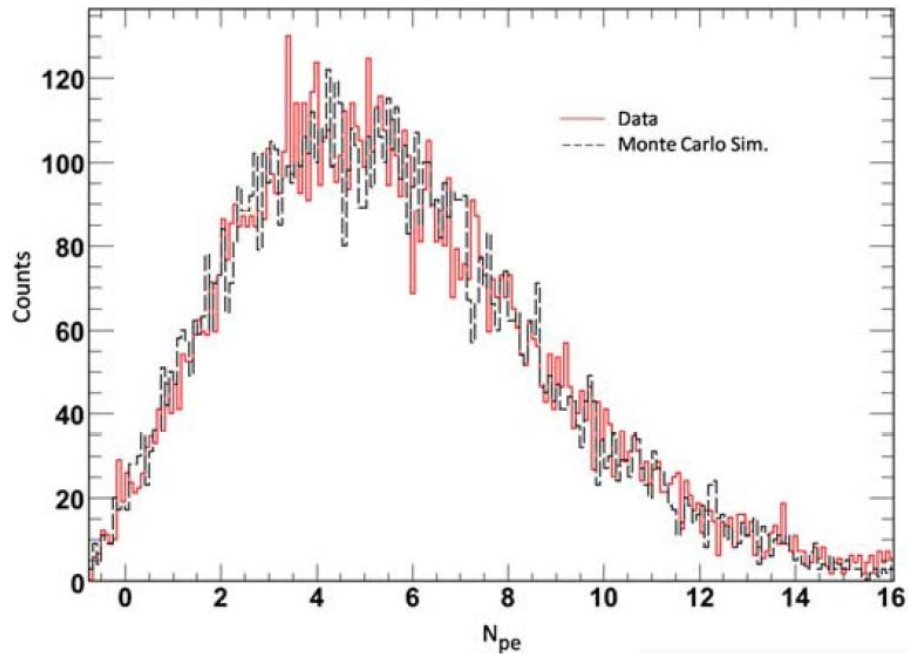


Figure 22: Fitting Method. Here is an overlay of a typical measured pulse height distribution and its corresponding Monte Carlo simulation. (Azmoun et al. 2010)

Geometric Acceptance

The geometric acceptance of the apparatus was checked by a Y-scan. This acted as a systematic check of the experiment as well as a check of the simulated geometric acceptances in Fig 9. Fig 23 shows the data plotted as red points and compares it to Fig 9. The data collected matches the shape and values of the simulations well.

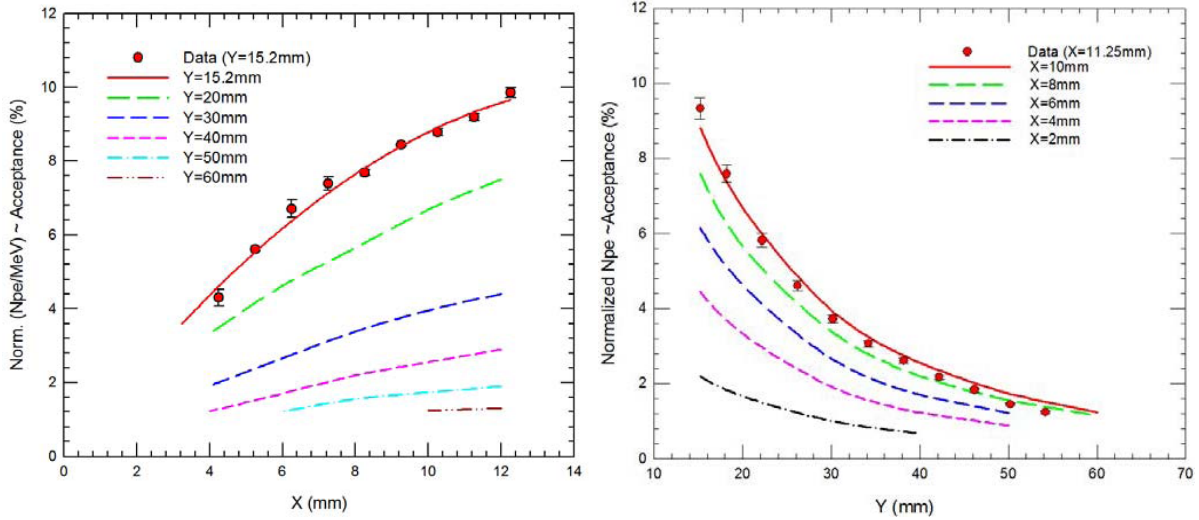


Figure 23: Geometric Acceptance Check. The points in red are the experimentally calculated geometric acceptance overlaid onto Fig 9.

Scintillation Light Yield per MeV of Deposited Energy

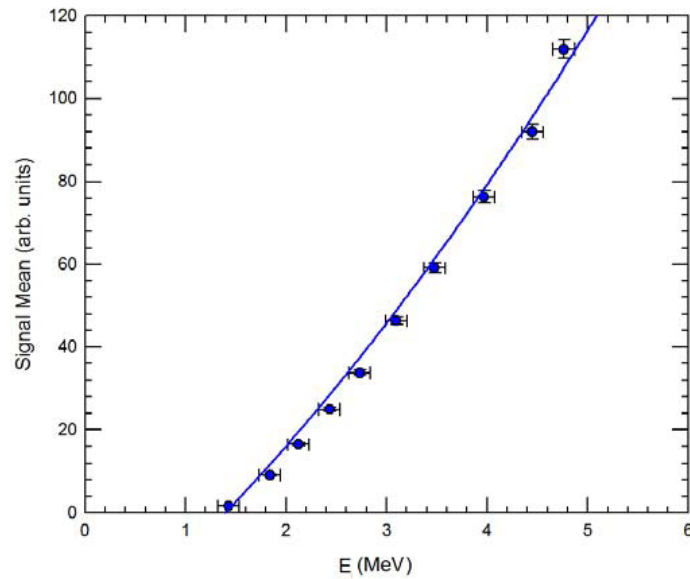


Figure 24: Mean Signal Output against the Energy Deposited. The data points of this figure are a result of the coupled signals received from the preamplifier and the energy of the alpha particles. This plot was produced before correcting for the geometric acceptance. The curve is a best fit of the data. (Azmoun et al. 2010)

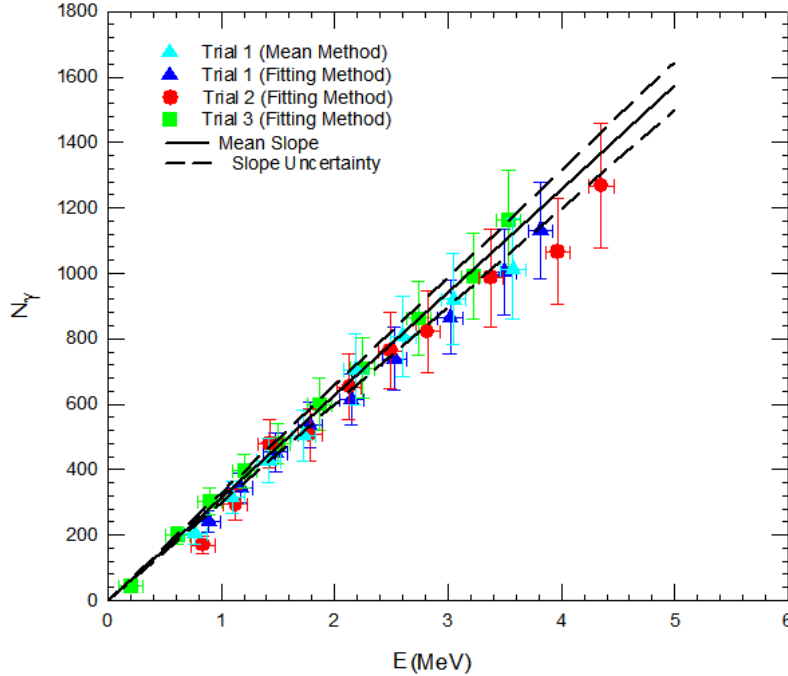


Figure 25: Absolute Scintillation Light Yield per MeV of Deposited Energy. The plot shown contains numerous trials of the experiment after correcting for the geometric acceptance. These trials agree well and the best fit slope is shown as well as its uncertainty, which includes systematic errors. (Azmoun et al. 2010)

After completing the procedure we result in a plot of the signal received from the preamplifier as a function of the energy deposited into the gas, Fig 24. The points are a result of the signal received from the preamplifier as a function of the energy deposited into the gas before correcting for the geometric acceptance. The offset seen is due to the scintillation light blocked by the collimating cylinder, the source holder, and the fixture holding the SBD. After correcting for the geometric acceptance, the offset decreased, and the curve became more linear. The offset was not accounted for by the Monte Carlo simulations used in the fitting method, however because we are calculating a linear slope, $\frac{dN_\gamma}{dE}$, the constant offset will not affect the final quantitative result corrected by the 4π solid angle,

Fig 25. Fig 25 depicts three trials using the fitting method and one trial using the mean method. It is visually apparent that the mean method is not as linear as the fitting method due to the gain fluctuations and noise pedestal; the fit is slightly lower than the fitting method as well. A linear fit was produced for

each trial and the overall slope is the weighted average, where $dN_{\gamma}/dE = 314 \pm 15$ number of photons per MeV of deposited energy. Adding a quadratic term did not affect the final value substantially. The uncertainty quoted includes systematic errors in the experiment.

Conclusion

This experiment measured the amount of scintillation light yield per MeV of deposited energy over at 4π solid angle to be 314 ± 15 photons per MeV of deposited energy in CF_4 . The pulse height distribution produced by the scintillation light was analyzed by two independent methods while simultaneously measuring the energy the alpha particles deposited into the gas. The alpha particles were emitted by an ^{241}Am source to scintillate the CF_4 and the scintillation light produced was absorbed by a CsI photosensitive cathode evaporated on the top GEM of a triple GEM stack. The photocathode produced photoelectrons which were amplified by the GEM stack and collected onto a readout pad. This signal traveled through a charge sensitive preamplifier and was collected on a digital oscilloscope and a ROOT data collection program. The spectrum produced by the oscilloscope was used to find the mean of the peak. The spectrum produced by the ROOT program was fit to a Poisson distribution according to the number of primary photoelectrons produced by the photocathode and was convoluted with a Gaussian distribution due to the noise pedestal and a Polya gain distribution due to gain fluctuations. Simultaneously, the energy of the alpha particles was measured with a Silicon SBD which allowed us to derive the amount of energy deposited into the gas as well as trigger the oscilloscope and ROOT program. The set of pulse height spectrums were analyzed independently, via two methods, to find the number of primary photoelectrons and were found to agree. The mean method used the mean of the spectrum and experimentally calculated gain of the triple GEM stack. The fitting method used the spectrum produced by the ROOT program which was best fit to a Monte Carlo simulation using a chi squared analysis. The Monte Carlo simulations were produced by varying the number of primary photoelectrons. The final measurement of $\frac{dN_\gamma}{dE}$ was a weighted average of a number of trials using both methods. The final calculation agrees well with previously calculated measurements as well as other measurements (Pansky et al. 1995), however the measurement found by this experiment is more precise and significantly improved.

References

- Leo WR. 1994. Techniques for Nuclear and Particle Physics Experiments. 2nd rev ed. New York: Springer-Verlag
- Fernow RC. 1986. Introduction to Experimental Particle Physics. 1st ed. London: Cambridge University Press
- Gernhäuser R et al. 1996. Photon Detector Performance and Radiator Scintillation in the HADES RICH. Nucl. Instr. And Meth. A 371: p. 300-304
- Bock RK, Vasilescu A. 1999. The Particle Detector BriefBook [Internet]. Geneva, Switzerland and Bucuresti, Romania: CERN. [cited 2010 Oct 22]. Available from: <http://rkb.home.cern.ch/rkb/titleD.html>
- Sauli F. 1997. GEM: A New Concept for Electron Amplification in Gas Detectors. Nucl. Instr. and Meth. A 386: p 531-534
- Azmoun B et al. 2010. A Measurement of the Scintillation Light Yield in CF₄ Using a Photosensitive GEM Detector. Nucl. Instr. and Meth. vol. 57(4): p 2376-2381
- Bachmann S et al. 1999. Charge Amplification and Transfer Process in the Gas Electron Multiplier. Nucl. Instr. and Meth. A 438: p 376-408
- Azmoun B et al. 2005. Conceptual Design Report on a HBD Upgrade for the PHENIX Detector [Internet]. Upton, NY: BNL. [cited 2010 Oct 22]. Available from: http://www.phenix.bnl.gov/WWW/TPCHBD/HBD_CDR.pdf
- Va'vra J et al. 1993. Measurement of Electron Drift Parameters for Helium and CF₄-Based Gases. Nucl. Instr. and Meth. A 324: p 113-126
- Kozlov A et al. 2004. Development of a Triple GEM UV-Photon Detector Operated in Pure CF₄ for the PHENIX experiment. Nucl. Instr. and Meth. A 523: p 345-354
- Gotoh S and Takagi Z. 1964. Silicon Surface Barrier Detector. Journal of Nucl. Sci. and Tech. vol. 1(8): p 311-315
- Woody C et al. 2009. Collection of Photoelectrons and Operating Parameters of CsI Photocathode GEM Detectors. IEEE Transactions on Nucl. Sci. vol. 56(3): p 1544-1549
- Evans R. 1955. The Atomic Nucleus. New York, New York :McGraw-Hill, Inc.
- Pansky A et al. 1995. The Scintillation of CF₄ and its Relevance to Detection Science. Nucl. Instr. and Meth. A 354: p 262-269